

Variation of atmospheric depth profile on different time scales

B. Wilczyńska^{a,*}, D. Góra^a, P. Homola^a, J. Pękala^a,
M. Risse^{a,b}, and H. Wilczyński^a

^a *Institute of Nuclear Physics PAN, ul.Radzikowskiego 152, 31-342 Kraków,
Poland*

^b *Forschungszentrum Karlsruhe, Institut für Kernphysik, 76021 Karlsruhe,
Germany*

Abstract

The vertical profile of atmospheric depth is an important element in extensive air shower studies. The depth of shower maximum is one of the most important characteristics of the shower. In the fluorescence technique of shower detection, the geometrical reconstruction provides the altitude of shower maximum, so that an accurate profile of atmospheric depth is needed to convert this altitude to the depth of shower maximum. In this paper the temporal variation of experimentally measured profiles of atmospheric depth at different sites is studied and implications for shower reconstruction are shown. The atmospheric profiles vary on time scales from hours to years. It is shown that the daily variation of the profile is as important as its seasonal variation and should be accounted for in air shower studies. For precise shower reconstruction, the daily profiles determined locally at the site of the air shower detector are recommended.

Key words: extensive air showers, atmospheric depth, shower maximum

PACS: 96.40.Pq

1 Introduction

The atmosphere is the key component of any detection system for extensive air showers. All cosmic rays with energies larger than about 10^{15} eV are detected via recording extensive air showers they initiate in the atmosphere. Details of

* *Correspondence to:* B. Wilczyńska (Barbara.Wilczynska@ifj.edu.pl)

shower development depend on the primary cosmic ray particle, but also on the properties of the atmosphere itself, in particular on the vertical distribution of mass in the atmosphere. Since the atmosphere serves both as a target in which primary cosmic rays interact and as the medium in which showers develop, a precise knowledge of relevant properties of the atmosphere is extremely important for studies of high energy cosmic rays.

Studies of the atmosphere done over decades have resulted in a fairly good knowledge of the distributions of atmospheric air. The atmospheric conditions are quantitatively described using parameters like temperature, pressure, wind speed etc. as a function of time and location. In contrast to many other areas of physics in which measurements and observations are performed in laboratory experiments and are well controlled and reproducible, the atmospheric phenomena are studied by observing natural processes which cannot be controlled by the observer. These atmospheric phenomena are reproducible only as much as is characteristic to the phenomena under study. For example, the temporal variation of temperature can be presented as a superposition of an average over many years, seasonal variations, diurnal variation and irregular variation of different time scales. Similarly one can use the spatial scale (vertical or horizontal) of the temperature field or of other parameters of interest.

The atmosphere is in a state very near the local hydrostatic equilibrium, i.e. the difference of atmospheric pressures between two levels is always close to the weight of a column of air with unit cross section. This results in a characteristic, near exponential, vertical distribution of pressure (and consequently of air mass) in the atmosphere. Generally, the atmospheric pressure (and the overlying mass) falls by an order of magnitude every 16–20 km, for altitudes up to 100 km.

Traditionally, the atmosphere is divided into layers, most commonly according to the vertical distribution of temperature. These layers are: *(i)* troposphere, in which temperature falls with increasing altitude, which extends up to altitudes of about 7 km near the poles or 16 km near the equator, *(ii)* stratosphere, up to about 50 km with approximately constant temperature (lower stratosphere) or increasing temperature (upper stratosphere), *(iii)* mesosphere, up to about 85 km, in which temperature falls again with altitude, *(iv)* thermosphere, where the temperature increases with altitude, and which extends up to the limit of atmosphere. The boundaries between these layers are called tropopause, stratopause and mesopause, respectively. Most of the mass of the atmosphere (about 75%) is contained in the troposphere; the troposphere and stratosphere combined contain more than 99% of the atmospheric mass.

The primary source of energy which drives the atmospheric phenomena is the radiation of the Sun. The local flux of incoming energy depends on geographic location, shape of the terrain, time of day and year and on transparency of

the air (i.e. cloudiness, pollution etc). Movements of air make the dependence on irradiation more complex, therefore observations and measurements of atmospheric phenomena must be done in many places to get a coherent picture of the atmosphere.

The main atmospheric parameter which governs the longitudinal development of an extensive air shower is the column depth of the air traversed by the shower over its pathlength l ("slant depth"): $X_{sl} = \int \rho(h)dl$, where $\rho(h)$ is the altitude-dependent air density. Therefore, for studies of air showers, the basic atmospheric parameter is the vertical profile of atmospheric depth: $X_V(h) = \int_h^\infty \rho(h)dh$, which provides a correspondence between the atmospheric depth X_V and altitude h above the sea level. For showers with not-too-large zenith angles, $\theta \leq 70^\circ$, the vertical and slant atmospheric depth are related by $X_{sl} = X_V / \cos \theta$. In the following, mainly the vertical atmospheric depth will be considered, so for simplicity X will be used instead of X_V , unless explicitly stated otherwise.

In studies related to development and detection of extensive air showers, the US Standard Atmosphere Model [1] is commonly used. This model provides distributions of temperature and pressure as functions of altitude. The 1976 extension of the Model provides also the northern mid-latitude winter and summer atmosphere distributions. An important question is, however, how well does the US Standard Atmosphere Model approximate local conditions at the sites of air shower detectors, and what is the time variability of the local atmosphere? In other words, is the annual or seasonal average adequate for a particular day at a particular location? This question is especially important for the fluorescence technique of shower detection. The depth of shower maximum, X_{max} , is the key parameter for identification of the primary particle of the shower. However, in the fluorescence detector the altitude h_{max} of shower maximum is determined from the geometry reconstruction and the corresponding atmospheric depth of the maximum has to be derived using an appropriate $X \leftrightarrow h$ relation. It is now well known [2,3,4,5,6] that a good knowledge of atmospheric depth profile is essential for precise shower reconstruction.

The global COSPAR International Reference Atmosphere (CIRA86) [7] provides temperature and pressure profiles at altitudes above 20 km at many latitudes at both hemispheres. However, most of the air shower development takes place at altitudes smaller than 20 km, so that the CIRA86 model is not sufficient for air shower studies.

The UK Met Office, through the British Atmospheric Data Centre, maintains a data base of measurements done by radiosondes at a number of locations worldwide [8]. A radiosonde is a small package of instruments, suspended from a helium-filled balloon. During ascent of the balloon the radiosonde measures

the temperature, pressure and humidity at intervals of typically 2 seconds. The information is transmitted via radio to the ground station, which processes and stores the data. The balloon typically reaches the altitude 20–30 km before it bursts and the radiosonde falls, being attached to a small parachute. The "standard resolution" data, which are used in this study, consist of radiosonde data read out at the standard pressure levels, which are: 1000, 925, 850, 700, 500, 400, 300, 250, 200, 150, 100, 70, 50, 30, 20 and 10 mbar.

In this paper, we present the results of a study of atmospheric profiles at Salt Lake City (USA), near the site of the HiRes experiment and at Mendoza (Argentina), near the site of the southern Pierre Auger Observatory. The studies are based on the Met Office data collected in daily balloon soundings of the atmosphere performed at the Salt Lake City and Mendoza airports.

2 Variation of temperature and pressure profiles

The variation of temperature with altitude in the US Standard Atmosphere Model is shown in Fig. 1 for annual mean as well as for winter and summer. The variation of actual measurements done at Salt Lake City in winter (average of January measurements over four years) and in summer (average of July) are also shown. The seasonal variation of temperature distribution is apparent. Although a similar behaviour of the temperature distributions in both the model and the measurements is observed, there are also considerable differences, which will be discussed below.

In the following, let's concentrate on fluctuations of the air temperature. Since the temperature of the air near the ground is strongly influenced by weather effects, choosing some higher altitude seems to be more representative for studies of the seasonal variation of the temperature distribution. We choose the altitude of 5.8 km above sea level (near the 500 mbar standard pressure level in the Met Office data set). The distribution of daily temperature at this altitude during the months of January and July is shown in Fig. 2. These come from soundings made at Salt Lake City during years 1999–2002. The average temperatures in January and July at 5.8 km altitude differ by 14 degrees. The variation of temperature in January is much larger than in July. The width of the distribution, especially for the January data, suggests that in addition to seasonal differences, the daily variation may also be important.

From the January Salt Lake City measurements, three extremely warm days (about 10 degrees warmer than average) were selected, to be compared with three cold days, with temperatures about 10 degrees lower than average. The temperature profiles of these selected days, shown in Fig. 3a and 3b, are quite distinct: a day warmer than average at altitude 5.8 km is colder than average

in the tropopause (above ~ 12 km) and vice versa. A "warm" day is consistently warmer than average over the whole troposphere and a "cold" day is consistently colder. The temperatures fall monotonically with altitude in the troposphere, with roughly the same rate of temperature decrease. We note that temperature inversions over small ranges of altitude are not visible in this standard resolution data set of measurements at relatively large intervals in altitude. The profiles of pressure as a function of altitude are shown in Fig. 3c and 3e for the same days. They also show systematic differences between warm and cold days. As a result of the temperature and pressure differences, the derived densities of air (see Section 3) differ significantly, as shown in Fig. 3d and 3f. As the atmospheric depth is the integral of density of the overlying air, it is clear that the profiles of the atmospheric depth will be distinctly different for cold and warm days.

As shown in Fig. 4, a similar pattern of temperature variation holds for cold and warm *seasons* (January and July) and for cold and warm *days* in any of these two seasons. Higher temperatures at the low altitudes imply lower temperatures in the tropopause. The same pattern is observed in Mendoza.

The inference one can make is that the daily variation of the atmosphere may be as important as the seasonal variation. If so, the seasonal and daily fluctuations of temperature and pressure may make the actual atmospheric depth profiles differ considerably from the average one, as will be shown below.

3 Determination of density and atmospheric depth profiles

The atmospheric depth at an altitude h is the integral of density of the overlying air: $X(h) = \int_h^\infty \rho(h)dh$. Since the air density is not measured directly, it must be inferred from the ideal gas law based on measurements of pressure p and temperature T :

$$\rho(p, T) = \frac{pM_{mol}}{RT} = 0.34839 \frac{p[mbar]}{T[K]} \left[\frac{g}{cm^3} \right], \quad (1)$$

where $M_{mol} = 28.966$ g/mol is the molar mass of air and $R = 8.31432$ J/(K mol) is the universal gas constant. In this work we use the pressure and temperature profiles measured by radiosondes up to the altitude of 20–30 km (as available). At higher altitudes, the CIRA86 model is used.

The atmospheric depth in the US Standard Atmosphere model in the CORSIKA shower simulation package [9] is parameterized in four altitude ranges

below 100 km by exponential functions

$$X_i = a_i + b_i e^{-h/c_i} \quad (2)$$

and by a linear function

$$X = a_5 - b_5 h/c_5 \quad (3)$$

for altitudes 100–112.8 km. This parameterization is widely used in shower simulation and reconstruction codes.

The exponential form of the atmospheric depth profile implies an exponential distribution of the air density $\rho(h)$. The average July and January distributions of density in Mendoza are shown in Fig. 5a and 5b (the distributions at Salt Lake City are very similar). The exponential distributions should be represented by straight lines in these semi-logarithmic plots. The data points show the actual average air density in summer and in winter. The dotted lines are just straight lines drawn between the first and last data points in each plot. It is evident that the data points do not follow a single exponential distribution, nor exponential distributions are seen in specific ranges of altitude (no straight sections are present in the plots). A clear inference is that the real atmospheric density distribution does not quite follow the exponential distribution in any wide range of altitudes.

To study the shape of the density distribution in more detail, the exponential function of the form

$$\rho(h) = b \exp(-h/c) \quad (4)$$

was fitted to every pair of adjacent data points. The variation of the parameter c (the scale height of the exponential distribution) is shown in Figures 5c and 5d. This parameter changes continuously with altitude, so fitting the exponential function in wide ranges of altitudes is only a more or less crude approximation of the true distribution. Therefore, the procedure for determining the atmospheric depth profile $X(h)$ should be the following. Instead of fitting the $\rho(h)$ function to the data points and integrating the $\rho(h)$ analytically to find $X(h)$, the atmospheric depth is determined by interpolating (with an exponential function of Eq. 4) the density between two adjacent data points and integrating the density from one data point to another. In this way, the obtained $\rho(h)$ distribution follows exactly the data points, and the uncertainties are due only to experimental errors of the data points, which are small. Assuming the measurement errors of temperature and pressure as quoted by the manufacturer of the radiosondes used, the resulting uncertainty of $X(h)$ turns out to be smaller than 2 g/cm² in the whole range of altitudes.

It is, however, convenient to use an analytical function to approximate the profile of air density (and consequently, atmospheric depth), as is commonly used (Eq. 2). The scale heights of the fits in the standard CORSIKA altitude ranges: 0–4 km, 4–10 km, 10–40 km and 40–100 km are shown in Fig. 5c and 5d by the dotted lines. It is evident that fits in other ranges can be more accurate. We choose fits in ranges: 0–7 km, 7–12 km, 12–30 km and 30–100 km, shown by the solid lines in 5c and 5d. Such "non-standard" ranges are allowed e.g. in CORSIKA. We note that the rather poor agreement of the fit with the data in the fourth range (above 30 km) has a negligible effect on air shower studies: the atmospheric depth at 30 km is only about 12 g/cm², so that showers develop mostly at lower altitudes.

4 Seasonal variation of atmospheric profiles

Given the large seasonal variation of the temperature profile discussed in Section 2, it is to be expected that the profile of atmospheric depth may also vary considerably. The seasonal variation of the atmospheric depth profile $X(h)$ at both sites analyzed (Salt Lake City and Mendoza) is shown in Fig. 6. To better show the details, the differences between the determined profiles and the US Standard Atmosphere model are plotted. Average profiles of single months chosen as representatives of each season are presented. A considerable seasonal variation is manifest, especially at Salt Lake City: the January and July profiles differ from each other by up to 20 g/cm² at Salt Lake City and by up to 10 g/cm² in Mendoza. At both sites the summer profile differs most from the US Standard Atmosphere model, and the winter profile is closest to it. The summer-winter variation is considerably larger at Salt Lake City than at Mendoza. It is to be noted that the US Standard Atmosphere Model is not adequate even for the annual average and would not represent an average local profile at either site. The seasonal profiles shown in Fig. 6 are averages of four years for the month indicated. However, the monthly averages vary year-to-year, as shown in Fig. 7. A monthly average determined in one year can differ from that determined in the next year by up to 10 g/cm². This year-to-year variation of the averages is a consequence of the daily variation, as discussed below.

5 Day-to-day variation

In addition to the seasonal variation of the atmosphere, a strong variation is observed on the time scale of days. In Fig. 8 the differences of the X distributions relative to the US Standard Atmosphere Model are presented for four

seasons in 2002 at Salt Lake City. Atmospheric profiles of individual days are shown for one month in each season. The range of profile variability changes with season: it is largest in winter and smallest in summer. In order to examine closer this variability, the individual days of January 2002 are shown in Fig. 9. The numbers near the lines denote the date of each day. The four-year average of January is shown by the heavy dashed line. One can note that the profiles of consecutive days differ typically by 3–5 g/cm², with profiles of consecutive days grouped together. Occasionally, a large change is observed from day to day, with differences exceeding 15 g/cm² (e.g. days 12–13, 18–19, 22–23). Most of days in the first decade of January lay above the monthly average, while in the rest of the month the profiles of days lay mostly below the monthly average. The deviation of a daily profile from the monthly average can also exceed 15 g/cm².

The character of daily variability in other seasons is very similar to that in winter, but the range of variability is smaller, as seen in Fig. 8. Therefore, the profiles of individual days in seasons other than winter are not explicitly shown here. The character of variation of daily profiles at other sites is similar to that at Salt Lake City. As an example, the daily profiles at Mendoza in winter and summer are shown in Fig. 10.

The data presented in this section demonstrate that taking into account only the seasonal variation of the atmosphere is not sufficient for precise shower reconstruction. The daily variation is equally important and should be accounted for. To illustrate this conclusion, the influence of seasonal and daily variation of atmospheric depth profiles on shower reconstruction is compared in Fig. 11. The altitude of shower maximum is shown for 10 EeV (=10¹⁹ eV) proton and iron showers, with the $X \leftrightarrow h$ conversion done using the extreme *seasonal* profiles (winter-summer) versus the extreme *daily* profiles *within a single month*. The day-to-day variation of the atmospheric profiles can be seen to be as important as the season-to-season variation. The variation of h_{max} due to fluctuations of daily profiles constitutes a large portion of the h_{max} difference between proton and iron showers, especially at Salt Lake City. One can conclude that not only the US Standard Atmosphere model is not sufficiently accurate, but using any *average* profile, even made specifically for a particular season at a given site, is not satisfactory. The daily, local soundings to determine the profile of atmospheric depth are recommended for precise determination of the position of shower maximum, and consequently, for identification of cosmic ray primaries.

6 Day-night variation

Observations of extensive air showers using the fluorescence technique can be done only during the night. However, some of the meteorological stations usually make balloon soundings during the day only. A question therefore arises whether one can calculate an accurate atmospheric depth profile for the night, based on the radiosonde data collected during the day. The station at Salt Lake City routinely makes two radiosonde soundings during the day (at 11.00 and 12.00 hours) and two soundings during the night (at 23.00 and 0.00 hours). The day-night atmospheric variation can therefore be studied at Salt Lake City.

The average (four-year) annual distributions of temperature and pressure for day and night are shown in Fig. 12 for January and July at Salt Lake City. The pressure distributions are practically identical, while the temperature shows considerable day-night difference near the ground (the temperature difference at altitudes around 30 km is not as important, as air shower development occurs mostly at lower altitudes). In July this temperature difference near ground is as large as 10 degrees. To demonstrate the day-night differences in profiles of atmospheric depth, the month of January 2002 will be used. Figure 13 shows the atmospheric depth distribution for first ten days of this month and for 10 nights following these days. The plot shows that the profiles of atmospheric depth generally evolve in a continuous way: in most cases a night profile lays between the profiles of the two neighbouring days. Therefore, interpolation between two consecutive days should reproduce the distribution for the night between these days reasonably well.

The comparison of the 'nightly' profiles interpolated from the neighbouring days and those actually measured during the night is shown in Fig. 14 for all nights in January and July 2002 at Salt Lake City. The differences between the interpolated profiles and those actually measured are not large: in most cases they are less than 5 g/cm². Figures 14b,d show the mean difference and its standard deviation as a function of altitude. It is evident that only at altitudes below about 2 km above the sea level, i.e. less than 1 km above the ground at Salt Lake City, the interpolated profiles differ appreciably from those actually measured. Therefore, it seems well justified that if soundings of the atmosphere made locally are not available for the night of interest, one can use the soundings made during the neighbouring days. The typical error introduced in this way is less than 3 g/cm² for altitudes above some 1 km above ground, although for individual days in winter it can exceed 5 g/cm².

7 Summary and conclusion

The vertical distribution of the atmosphere undergoes large variation at various time scales. Not only the US Standard Atmosphere model, but also any other static model, turn out to be poor approximations of the true state of the atmosphere. The systematic differences in atmospheric depth between the model and the actual value can exceed $X_V = 20 \text{ g/cm}^2$. The experimentally determined atmospheric profiles depend on the geographic location, with a different size of seasonal variation at different sites. The seasonal averages fluctuate from year to year. An average profile for a particular month can vary from year to year by as much as 10 g/cm^2 .

The deviation of a particular day's profile from the monthly average can be as large as 15 g/cm^2 . Although the profiles evolve more or less continuously from day to day, occasionally a large change, on order of 15 g/cm^2 , occurs between consecutive days. The daily variation of the atmospheric profiles is therefore as important as the seasonal variation, and depends on the geographic location.

The day-night variation appears to be rather small, with the standard deviation of about 3 g/cm^2 , and for specific days the difference can exceed 5 g/cm^2 .

It is to be remembered that the differences in the atmospheric depth quoted above concern the *vertical* profiles $X_V(h)$. For real showers, the differences are augmented by the factor $1/\cos\theta$, where θ is the zenith angle of the shower.

A clear conclusion emerges from these results: using a global model, such as the US Standard Atmosphere, introduces large errors and should be avoided. The daily variation of the atmospheric depth profile is as important as the seasonal variation. For a precise shower reconstruction, the atmospheric depth profile should best be determined locally, near the site of the shower detector, during the night of interest. If the nightly sounding is not available, an interpolation between consecutive days provides a reasonably accurate approximation. Only when daily profiles are not available, using monthly averages is advisable, with the caveat that the additional uncertainty introduced to shower reconstruction can reach even $\Delta X_V \approx 15 \text{ g/cm}^2$, depending on the season.

If the seasonal averages have to be used, one should note that the traditional division of the year into four 3-month seasons may not be the best choice. As an illustration, in Fig. 15 the monthly profiles (4-year averages) are shown for Salt Lake City and Mendoza. At both sites the profiles of four winter months (December–March at Salt Lake City and June–September at Mendoza) are close to each other. Thus from the point of view of shower reconstruction, these four months constitute the winter season. Similarly, the summer months might be July–August at Salt Lake City and December–March at Mendoza.

The parameterization of these monthly profiles is given in Tables 1 and 2: the parameters of the exponential functions of Eq. 2 are given in ranges of altitude h : 0–7 km, 7–12 km, 12–30 km and 30–100 km. These parameterizations approximate the monthly averages reasonably well, with the typical deviation from the data on the order of 2 g/cm². However, one should keep in mind that when using the monthly averages, the daily variation of the atmosphere (not accounted for) is the main source of uncertainties.

Acknowledgements. We thank Hans Klages, Ralph Engel and Bianca Keilhauer for useful discussions. This work was partially supported by the Polish Committee for Scientific Research under grants No. PBZ KBN 054/P03/2001 and 2P03B 11024 and in Germany by the DAAD under grant No. PPP 323. MR is supported by the Alexander von Humboldt Foundation.

References

- [1] US Standard Atmosphere Model,
http://nssdc.gsfc.nasa.gov/space/model/atmos/us_standard.html
- [2] B.Keilhauer et al., Astropart. Phys. 22, 249 (2004)
- [3] B.Wilczyńska et al., Proc. 28th ICRC, Tsukuba, 2, 571 (2003)
- [4] B.Keilhauer et al., Proc. 28th ICRC, Tsukuba, 2, 879 (2003)
- [5] J. Blümer et al., Proc. 29th ICRC, Pune, (2005)
- [6] B.Wilczyńska et al., Proc. 29th ICRC, Pune, (2005)
- [7] COSPAR International Reference Atmosphere,
<http://nssdc.gsfc.nasa.gov/space/model/atmos/cospar1.html>
- [8] The British Atmospheric Data Centre,
<http://badc.nerc.ac.uk/data/radiosglobe/radhelp.html>
- [9] D.Heck et al., Report FZKA 6019, Forschungszentrum Karlsruhe (1998)

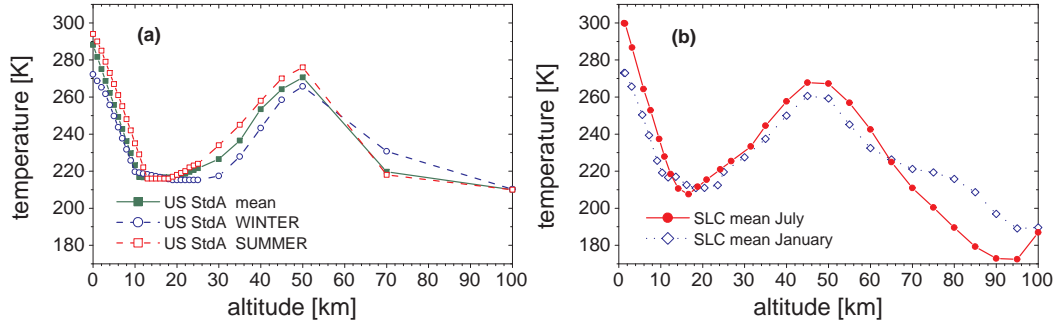


Fig. 1. Temperature dependence on altitude in (a) the US Standard Model and (b) averages of measurements done in January and July at Salt Lake City.

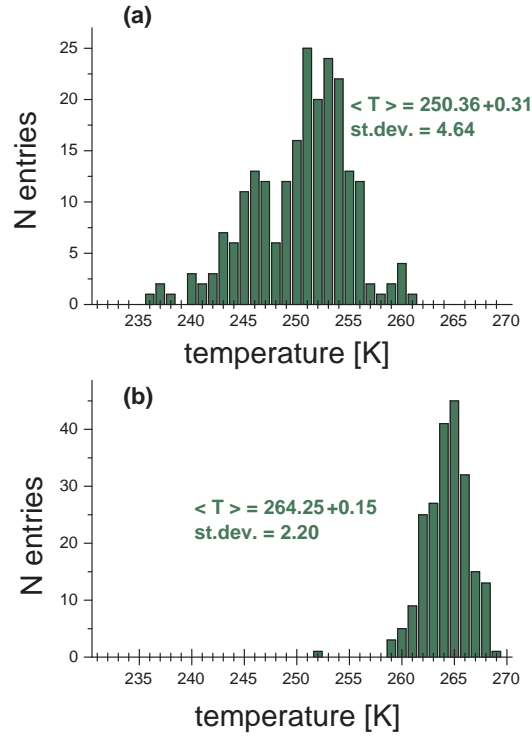


Fig. 2. Temperature distribution in (a) January and (b) July at altitude 5.8 km at Salt Lake City.

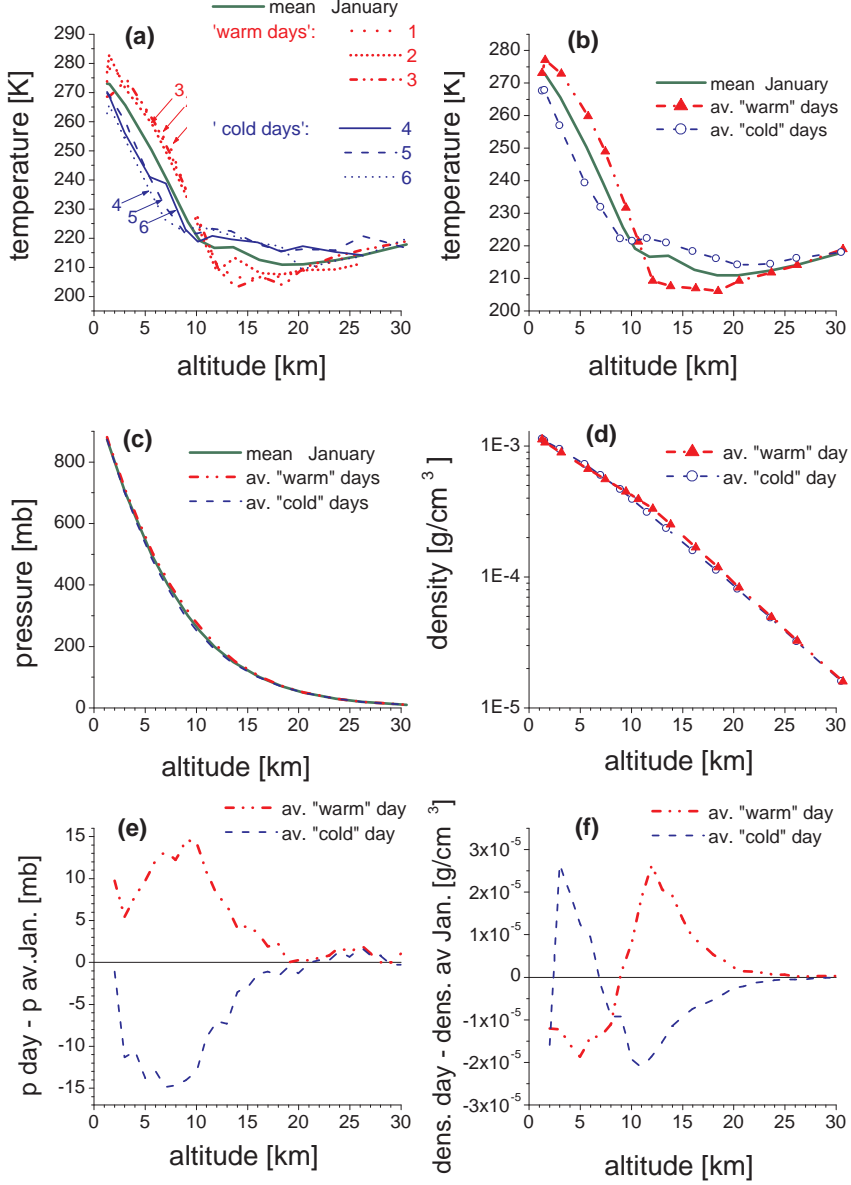


Fig. 3. (a, b) Temperature and (c) pressure distributions in three extremely warm and three extremely cold days in January at Salt Lake City. (d) Average air density in warm and cold days. (e) Differences in pressure distributions and (f) differences in density distributions of warm and cold days relative to the monthly averages.

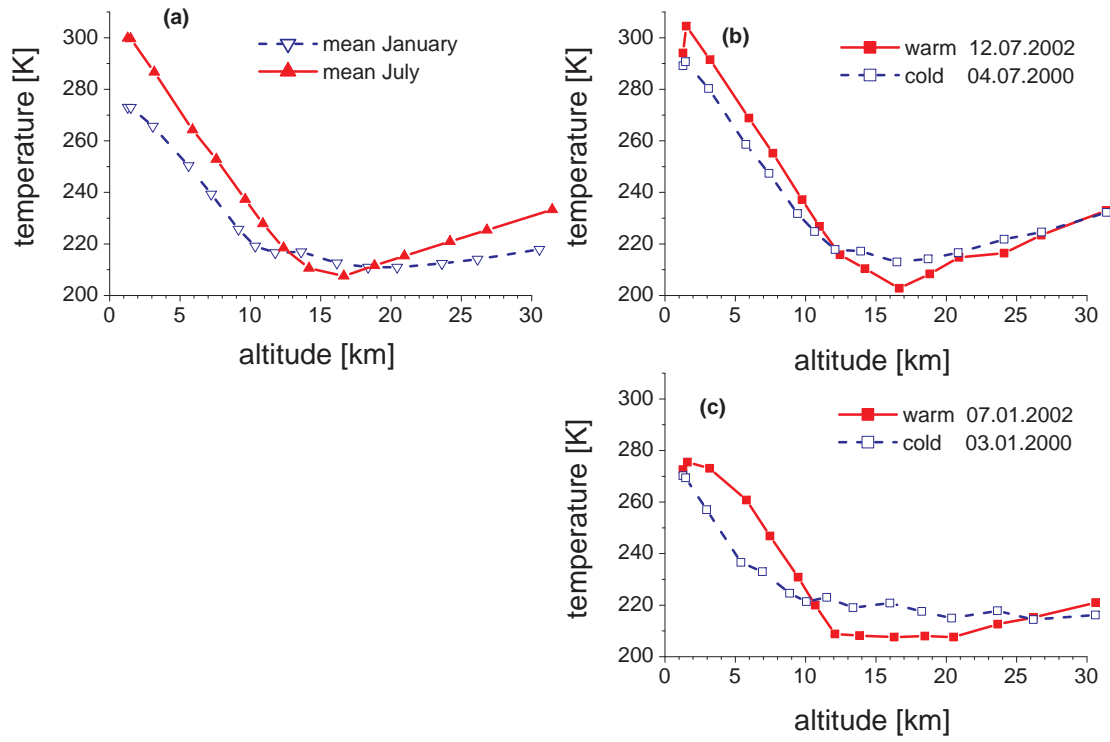


Fig. 4. Comparison of temperature distribution in cold/warm seasons to cold/warm days at Salt Lake City.

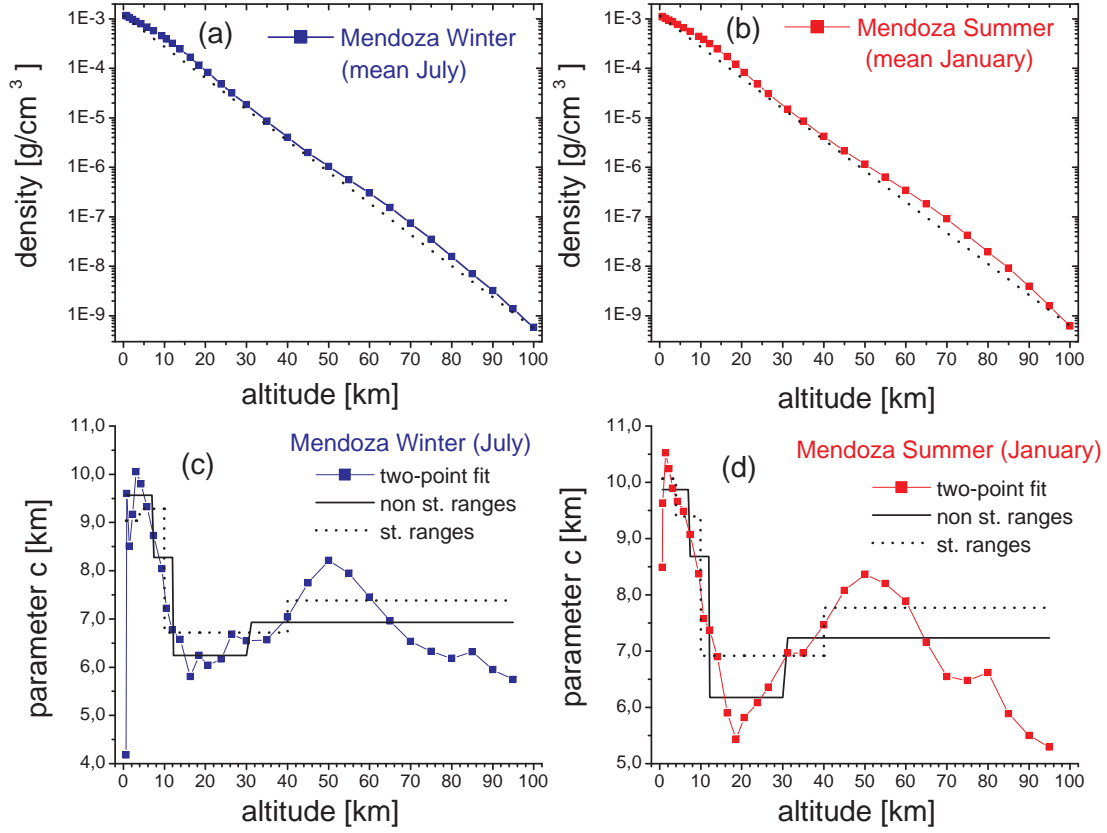


Fig. 5. Distribution of air density in (a) winter and (b) summer at Mendoza. In panels (c) and (d) the scale height parameter c , determined from the two-point fits (Eq.4) is compared to the four-exponent fits (Eq.2) in the standard altitude ranges (dotted lines) and in the chosen non-standard ranges (solid lines).

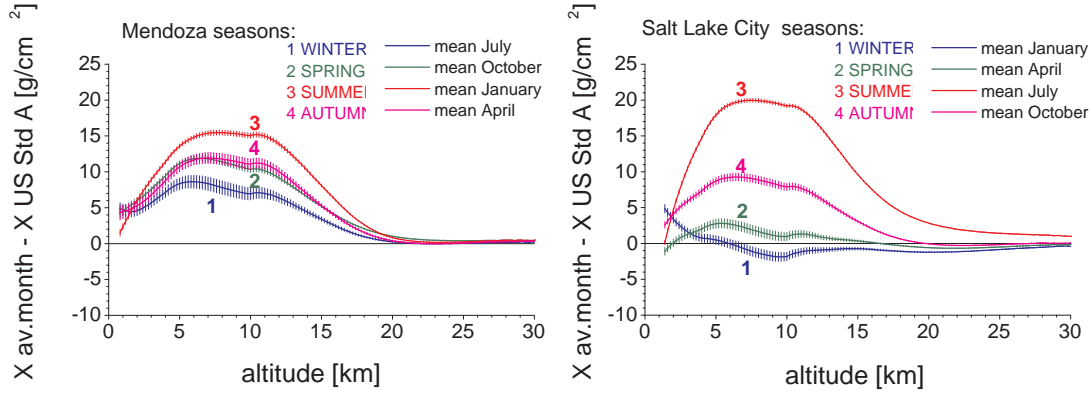


Fig. 6. Average seasonal atmospheric depth profiles, relative to the US Standard Atmosphere, at Mendoza (Argentina) and Salt Lake City (USA). The error bars represent the uncertainties of the average profiles.

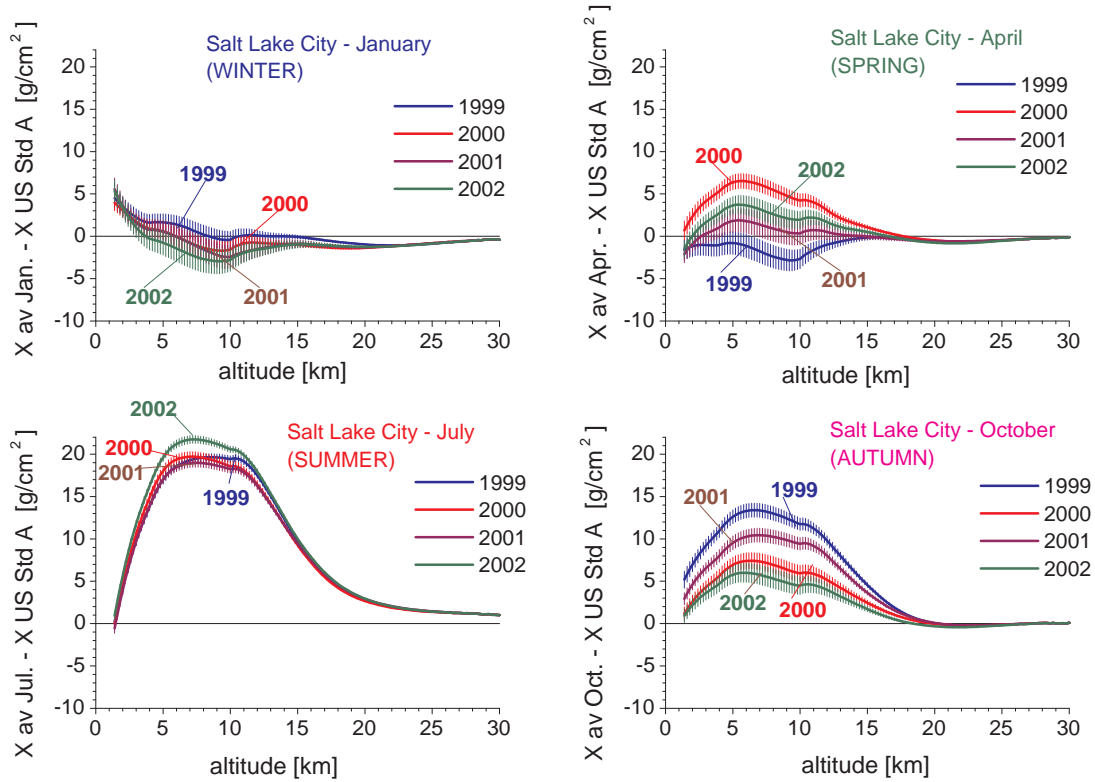


Fig. 7. Year-to-year variability of monthly average profiles at Salt Lake City. The error bars represent the uncertainties of the average profiles.

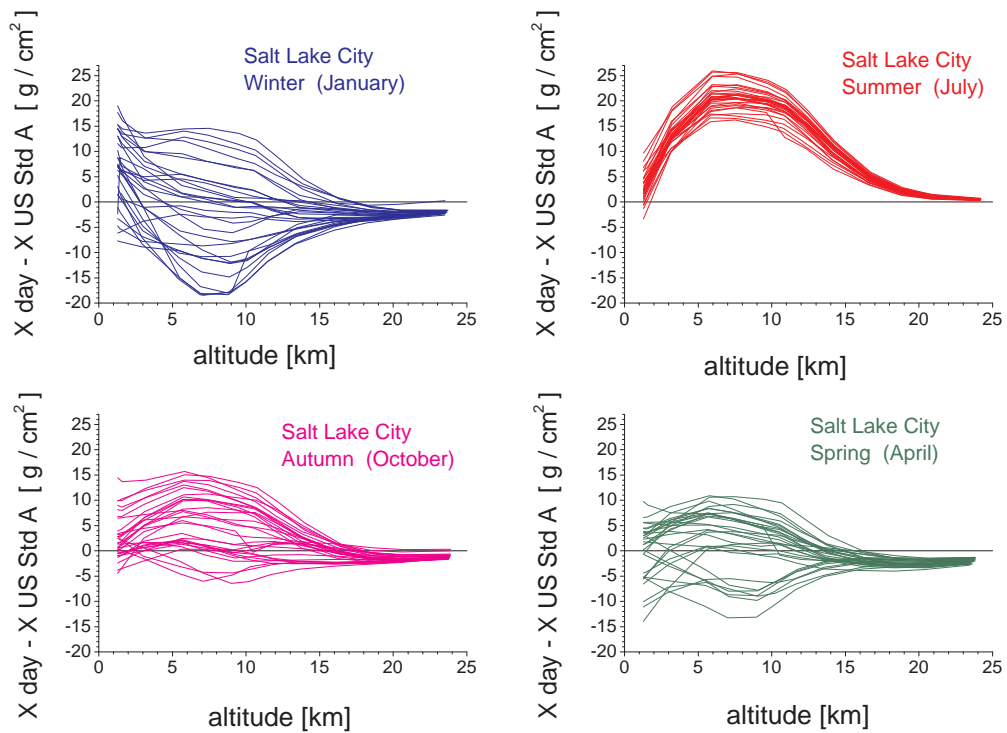


Fig. 8. Daily profiles of atmospheric depth relative to US Standard Atmosphere in four months of 2002 at Salt Lake City.

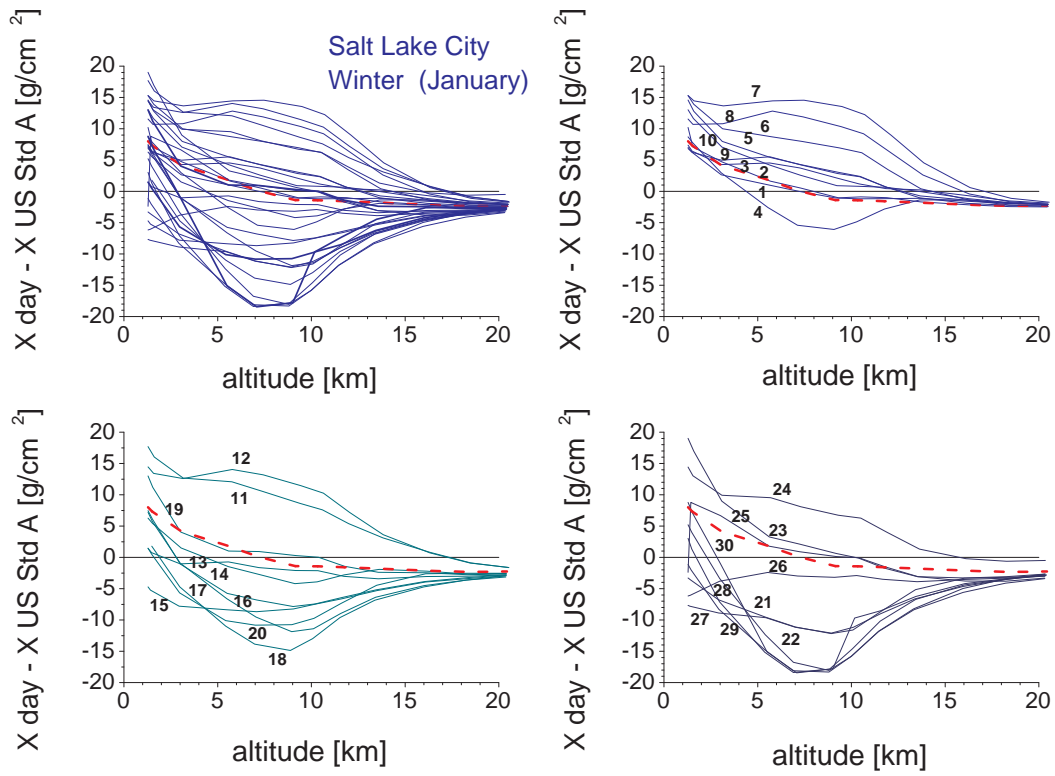


Fig. 9. Daily profiles of atmospheric depth relative to US Standard Atmosphere for January 2002 at Salt Lake City (upper left). The remaining panels show first, second and third decade of this month separately. The numbers indicate dates of individual profiles. The heavy dashed line represents the monthly average.

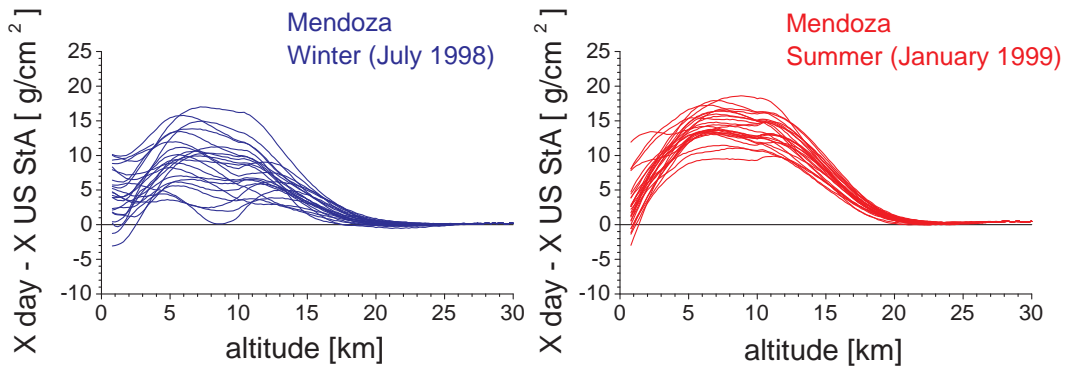


Fig. 10. Daily variation of atmospheric profiles in winter and summer at Mendoza.

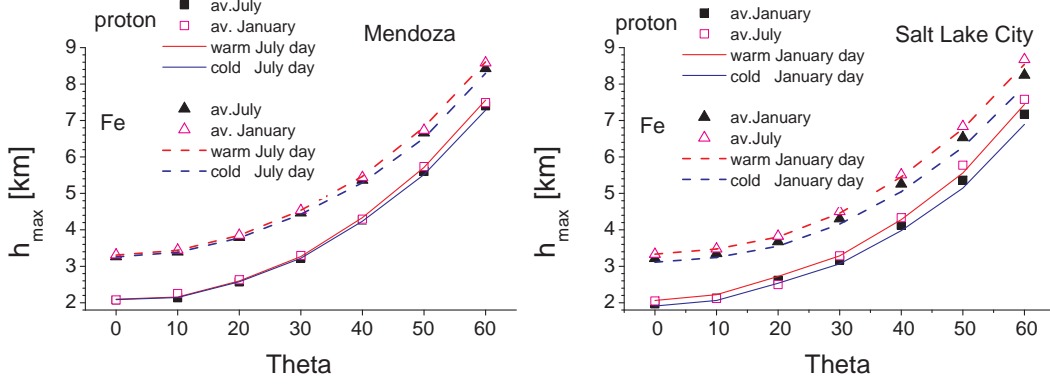


Fig. 11. Influence of seasonal and daily variation of atmospheric depth profiles on average altitude of shower maximum of 10 EeV proton and iron showers as a function of the shower zenith angle. The data points show altitudes of shower maximum in extreme seasons (winter and summer), while the lines represent the extremely warm and cold days in the corresponding single winter month.

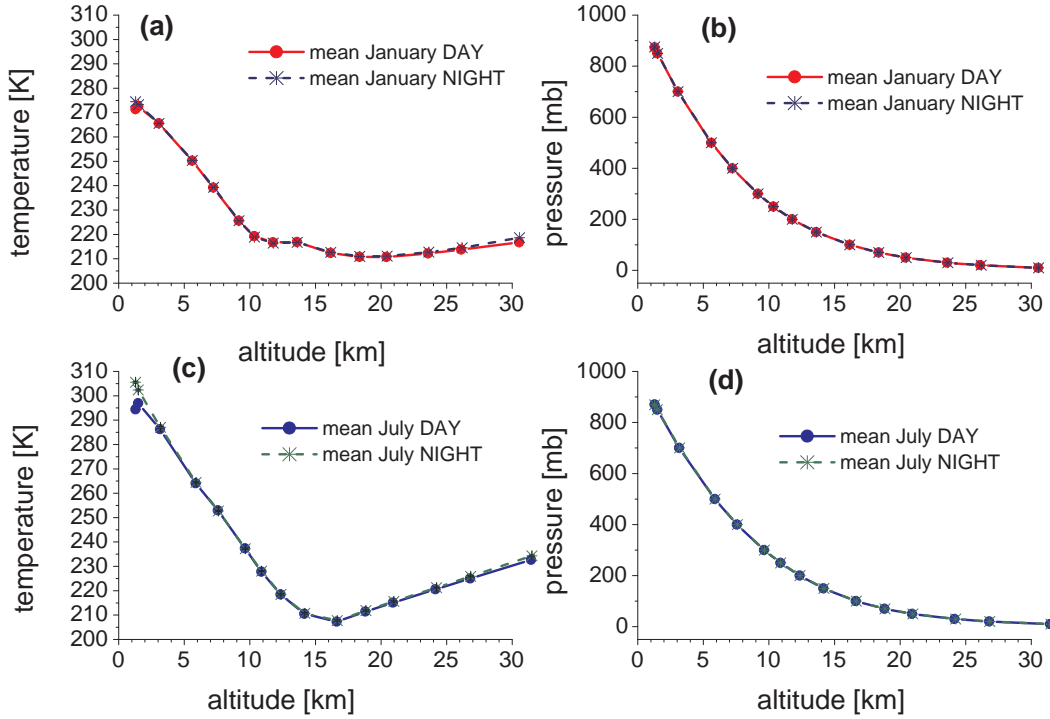


Fig. 12. Average monthly profiles of temperature and pressure measured during day and during night in January and July at Salt Lake City.

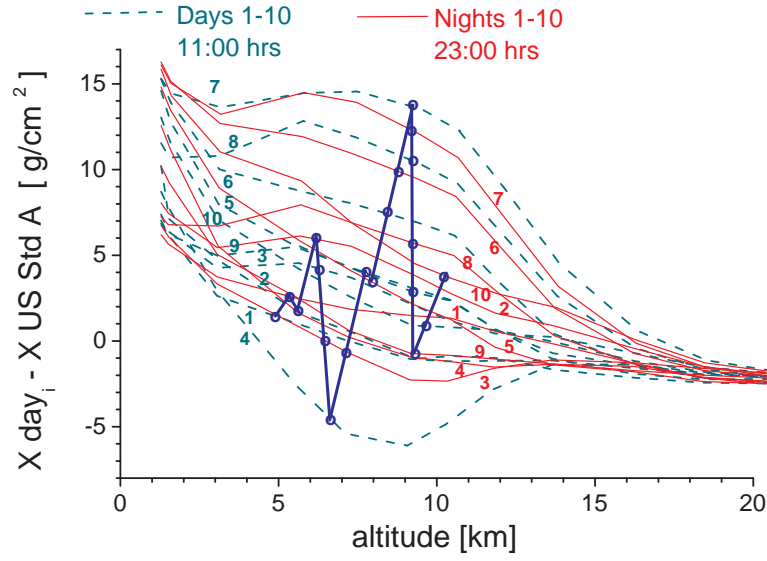


Fig. 13. Profiles of atmospheric depth measured in the first 10 days (dashed lines) and first 10 nights (thin solid lines) of January 2002 at Salt Lake City. The numbers indicate dates. The heavy solid line shows the sequence of consecutive day and night profiles.

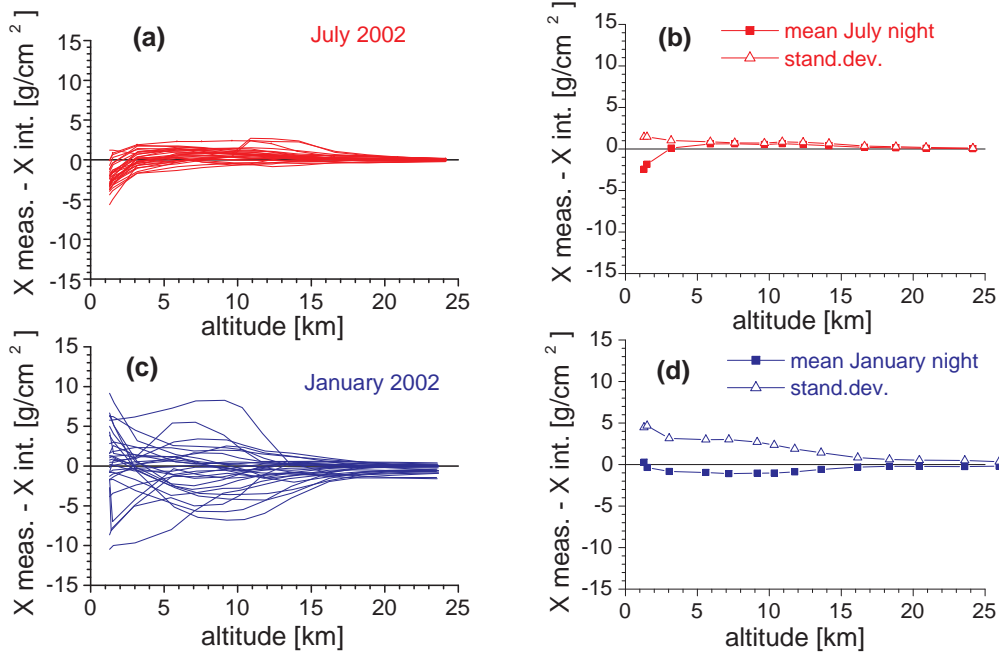


Fig. 14. (a, c) Differences between measured and interpolated nightly profiles of atmospheric depth in summer and winter at Salt Lake City. (b, d) Mean and standard deviation of profiles shown in (a) and (c).

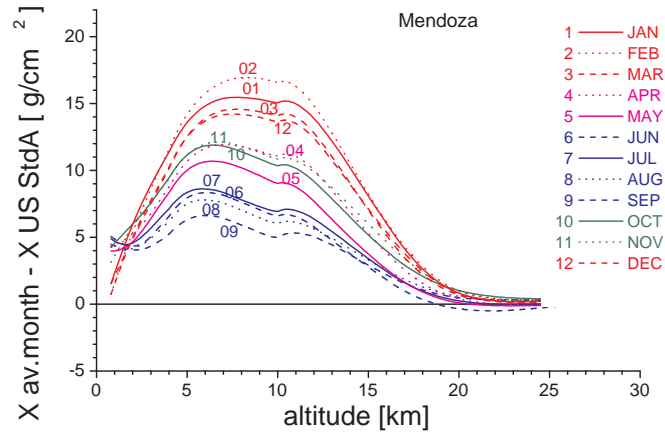
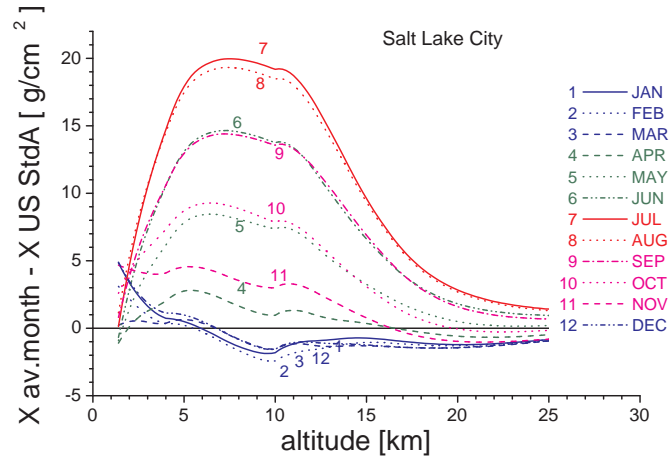


Fig. 15. Average monthly profiles of atmospheric depth at Salt Lake City and Mendoza.

Table 1

Parameters of fits to Eq.2 for annual and monthly averages of January–June at Mendoza and Salt Lake City.

Month	altitude km	Mendoza			Salt Lake City		
		a_i (g/cm ²)	b_i (g/cm ²)	c_i (cm)	a_i (g/cm ²)	b_i (g/cm ²)	c_i (cm)
av. year	0–7	-135.3657	1173.5795	964481.07	-150.5405	1186.6019	975370.45
	7–12	-71.2233	1148.3744	849610.95	-67.6044	1149.0158	833226.65
	12–30	1.2055	1429.8293	621337.57	0.9984	1388.8984	624933.79
	30–100	0.0106	870.8015	708709.48	0.0107	872.0169	705528.85
January	0–7	-143.1356	1179.0132	986940.77	-124.0319	1170.7336	913948.11
	7–12	-73.9046	1144.1639	868109.44	-52.5789	1150.1929	787455.67
	12–30	1.2702	1479.2616	617703.59	0.5428	1319.9111	631652.82
	30–100	0.0105	806.3091	723598.11	0.0108	887.3348	696567.06
February	0–7	-135.9059	1170.4334	982287.73	-132.5538	1176.2907	926334.89
	7–12	-83.9765	1144.0362	892118.25	-53.1326	1152.4537	786177.03
	12–30	1.4610	1497.6338	614675.42	0.4332	1311.1860	632894.01
	30–100	0.0105	809.6089	723681.98	0.0108	876.8543	697419.09
March	0–7	-133.5557	1169.3232	972625.45	-145.2204	1183.7779	948368.62
	7–12	-77.3797	1144.7436	872448.79	-59.3777	1151.4365	800062.39
	12–30	1.4111	1477.8039	615783.26	0.7382	1331.2019	627787.50
	30–100	0.0106	851.9467	713538.03	0.0107	829.3134	707135.34
April	0–7	-124.4756	1164.0947	950839.84	-158.6882	1193.1643	974561.42
	7–12	-73.4197	1147.2795	856075.22	-60.4142	1150.4190	807551.59
	12–30	1.3443	1448.0295	617898.74	0.7418	1337.5534	630095.46
	30–100	0.0107	896.5384	703568.67	0.0106	802.2364	716323.66
May	0–7	-136.2964	1174.7211	962756.90	-163.3301	1194.5484	998423.61
	7–12	-75.1491	1152.7025	851469.53	-73.3103	1148.9595	846457.10
	12–30	1.2284	1426.3171	618974.94	1.2485	1393.7719	624157.30
	30–100	0.0107	918.3066	697152.59	0.0105	803.1666	722517.74
June	0–7	-128.8113	1169.5907	945622.84	-172.3404	1200.2392	1028838.67
	7–12	-68.7814	1151.9990	834385.28	-82.4338	1149.3884	878122.45
	12–30	1.2704	1409.3793	619897.12	1.5904	1443.0171	621147.73
	30–100	0.0108	961.9427	689571.21	0.0104	817.2777	725898.04

Table 2

Parameters of fits to Eq.2 for monthly averages of July–December at Mendoza and Salt Lake City.

Month	altitude km	Mendoza			Salt Lake City		
		a_i (g/cm ²)	b_i (g/cm ²)	c_i (cm)	a_i (g/cm ²)	b_i (g/cm ²)	c_i (cm)
July	0–7	-137.0555	1177.1753	956627.92	-186.6534	1212.2804	1063017.00
	7–12	-64.9589	1151.1233	827880.59	-84.8974	1149.8003	894551.28
	12–30	1.0641	1395.2895	624326.08	1.6325	1487.4886	619070.90
	30–100	0.0108	944.3901	693374.71	0.0105	865.8201	718581.76
August	0–7	-134.8719	1174.8045	952297.63	-180.1574	1207.9734	1050566.85
	7–12	-63.5567	1151.4517	823187.06	-83.3827	1150.0202	889764.14
	12–30	0.9910	1371.1796	628951.14	1.4645	1478.0912	620467.75
	30–100	0.0107	921.2122	699108.09	0.0106	892.6000	711914.74
September	0–7	-130.0794	1171.1373	942652.20	-163.0811	1193.8657	1013663.92
	7–12	-60.0068	1150.2624	814932.30	-77.4142	1148.1548	868479.61
	12–30	1.1616	1368.4099	628284.06	1.1586	1439.6748	623016.99
	30–100	0.0107	903.4670	703442.29	0.0107	898.7723	705833.25
October	0–7	-138.3774	1177.5028	967536.19	-146.6575	1183.5344	973580.38
	7–12	-71.6140	1151.7126	847818.42	-74.4407	1150.8957	848663.14
	12–30	1.1403	1414.0158	624388.32	1.1837	1417.8501	619323.37
	30–100	0.0106	870.0336	709894.94	0.0108	921.7123	695498.81
November	0–7	-140.1651	1178.5255	971957.76	-131.1912	1174.5426	936106.26
	7–12	-69.6025	1149.7162	846709.27	-63.3954	1149.1226	817832.83
	12–30	0.8541	1412.1573	626853.42	0.6643	1377.7564	623196.00
	30–100	0.0105	809.6100	721090.69	0.0109	983.9849	678655.75
December	0–7	-143.6484	1178.6584	985389.83	-125.1286	1171.2049	916604.22
	7–12	-75.3706	1145.6133	867024.95	-56.5295	1151.9447	794149.64
	12–30	1.2267	1460.0256	619529.43	0.5446	1330.9703	628346.13
	30–100	0.0104	790.1251	726748.15	0.0108	932.9255	686075.79